Supporting information

Mechanism of SOA formation determines magnitude of radiative effects

Jialei Zhu[a], Joyce E. Penner[a], Guangxing Lin[b], Cheng Zhou[a], Li Xu[c],

Bingliang Zhuang[d]

a Department of Climate and Space Sciences and Engineering, University of Michigan, Ann Arbor, Michigan 48109, USA

b Pacific Northwest National Laboratory, Richland, Washington 99354, USA

c Department of Earth System Science, University of California, Irvine, CA, 92697, USA

d School of Atmospheric Sciences, Nanjing University, Nanjing, Jiangsu Province 210023, China

SI Text

S1. The method used to distribute SOA to pre-existing aerosols

SOA formation includes thermodynamic formation, kinetic formation and aqueous phase formation. Twenty-six different semi-volatile species are formed in the model which partition to the aerosol phase using the thermodynamic approach. The rate of formation of this SOA was proportional to the pre-existing organic aerosol mass as shown in the following two equations:

$$\frac{d\,SOA_{xSoot}}{dt} = \frac{M_{xOC}+M_{SOAxSoot}}{M_{OC}+M_{SOA}} \times \left(\frac{d\,evSOA}{dt} + \frac{d\,neSOA}{dt}\right) \quad (1)$$

$$\frac{d\,SOA_{nonSoot}}{dt} = \frac{M_{SOAnonSoot}}{M_{OC}+M_{SOA}} \times \left(\frac{d\,evSOA}{dt} + \frac{d\,neSOA}{dt}\right) \quad (2)$$

Here, SOA_{xSoot} is the mass concentration of SOA condensed on xSoot and xSoot stands for soot from either biomass burning (bSoot) or fossil fuel burning (fSoot). M_{xOC} is the mass concentration of organic carbon (OC) in xSoot and $M_{SOAxSoot}$ is the mass of SOA condensed on xSoot. M_{OC} is the total mass concentration of OC in soot. M_{SOA} is the total mass concentration of SOA condensed on all aerosols. evSOA and neSOA are SOA formed from traditional gas-particle partitioning (i.e. thermodynamic formation) and low-volatility SOA formed from irreversible aerosol-phase reactions of evSOA.

$SOA_{nonSoot}$ is the mass concentration of SOA condensed on the other aerosols except for soot, which could be sulfate, dust and sea salt in each mode or bin separately. $M_{SOAnonSoot}$ is the mass concentration of SOA condensed on these other kinds of aerosol. SOA formed from the kinetic approach includes SOA from IEPOX produced from the oxidation of isoprene, and oligomers from the uptake of gloyxal and methylglyoxal onto sulfate aerosols. This category of SOA was formed proportional to the pre-existing pure-sulfate aerosol area concentrations.

$$\frac{d\,SOA_{SO4i}}{dt} = \frac{S_{SO4i}}{S_{SO41}+S_{SO42}+S_{SO43}} \times \left(\frac{d\,neIEPOX}{dt} + \frac{d\,oligomers}{dt}\right) \quad (3)$$

Where $SO4_i$ is the sulfate aerosol in the nucleation/Aitken/accumulation mode. SOA_{SO4i} is the mass concentration of SOA condensed on $SO4_i$. S_{SO4i} is the surface area concentration (m^2/m^3) of $SO4_i$.

SOA formed through aqueous phase reactions in cloud water are organic acids in our model. They were distributed to all aerosols based on the number of cloud condensation nuclei (CCN) that can be formed by each kind of aerosol. The particle size, scavenging efficiency, refractive indices and hygroscopicity were all updated associated with the internal mixing of SOA.

S2. Differences in SOA burden in IM and IM_OC

The average burden of SOA decreases by -0.103 mg m^{-2} (4.8%) in the IM_OC scheme with a maximum decrease in tropical Africa of -0.613 mg m^{-2} due to the large emissions of bSoot there (Fig. S2). There is also a large decrease of the SOA burden in Eastern China, due to its high burden of fSoot. As noted in the main text, a large quantity of the SOA that was internally mixed with soot is instead mixed with sulfate in the accumulation mode, which also results in an increase in the hygroscopicity and particle size. This explains the decrease of wet and dry deposition especially in the regions where there are high concentrations of SOA associated with soot. There is also a small decrease of deposition in ocean areas caused by the smaller transport of SOA to these regions. In consequence, the burden of SOA in the IM_OC scheme is less than that in the IM scheme in all areas.

S3. Differences in DRE between IM and IM_OC.

Comparing the DRE due to SOA between IM and IM_OC, the assumption of no partitioning to primary OC decreases the DRE by 0.031 W m^{-2} (Fig. S4). If there is no partitioning of SOA to primary OC, the amount of SOA mixed with soot is reduced, thereby increasing the mass fraction of absorbing material within the soot (because soot is more absorbing than SOA). Also, the amount of SOA mixed with sulfate is increased, leading to an increase in the fraction of absorbing material mixed with sulfate. When the mass fraction of absorbing material increases there is a decrease in the absorption coefficient. As a result, the overall absorption by SOA is reduced in almost all areas (Fig. S5) and the cooling effect of SOA is increased. Nevertheless, the global average reduction of the SOA burden in IM_OC reduces its scattering which weakens the DRE (i.e. a smaller cooling effect). The net effect of these two opposing effects, leads to a reduction of the DRE in most regions in IM_OC, because of the decrease in SOA burden, and results in a stronger DRE in places with a larger decrease of absorption, such as in the middle of Africa and Eastern China (Fig. S4). However, the difference between IM_OC and IM is relatively small, ranging between -0.105 to 0.125 W m^{-2}.

S4. Differences in AIE between IM and IM_OC.

The CDNC increases when SOA is internally mixed with small particles in the IM_OC, allowing them to grow to CCN size. On the other hand, the CDNC will decrease when SOA is internally mixed with soot in IM and is condensed on larger particles which were already CCN. The difference in the AIE between IM and IM_OC results from the competition of these two mechanisms. The AIE in IM_OC is larger (more negative) in most in the coastal areas of middle South America and

South Africa by about -0.029 W m^{-2} while the AIE is decreased most in Southern Asia by 0.075 W m^{-2} (Figure S4).

S5. Other studies of indirect radiative effects of SOA.

Previous studies quantifying the radiation effects of SOA are limited and show a large range, especially for AIE. *Goto et al.* (1) estimates that the present day AIE due to SOA from monoterpenes is -0.19 W m^{-2} using an external mixing treatment for SOA, which treats aerosol mass only and neglects the number size distribution. *O'Donnell et al.* (2). used a thermodynamic approach to partition semi-volatile products and found a positive effect of +0.23 W m^{-2}. *Rap et al.* (3) assumed that monoterpenes form SOA with a fixed yield and the initial size distribution, which resulted with AIE of -0.02 W m^{-2}. *Scott et al.* (4) used the kinetic approach, assuming non-volatile organic material condenses irreversibly onto existing aerosol according to their Fuchs–Sutugin-corrected surface area, and accounted for new organic particle formation and estimated an AIE for SOA with -0.77 W m^{-2}. The uncertainty in the magnitude is partly associated with the different schemes applied for the formation of SOA in different models.

References

1. Goto D, Takemura T, & Nakajima T (2008) Importance of global aerosol modeling including secondary organic aerosol formed from monoterpene. Journal of Geophysical Research 113(D7).
2. O'Donnell D, Tsigaridis K, & Feichter J (2011) Estimating the direct and indirect effects of secondary organic aerosols using ECHAM5-HAM. Atmospheric Chemistry and Physics 11(16):8635-8659.
3. Rap A, et al. (2013) Natural aerosol direct and indirect radiative effects. Geophysical Research Letters 40(12):3297-3301.
4. Scott CE, et al. (2014) The direct and indirect radiative effects of biogenic secondary organic aerosol. Atmospheric Chemistry and Physics 14(1):447-470.

SI Figures

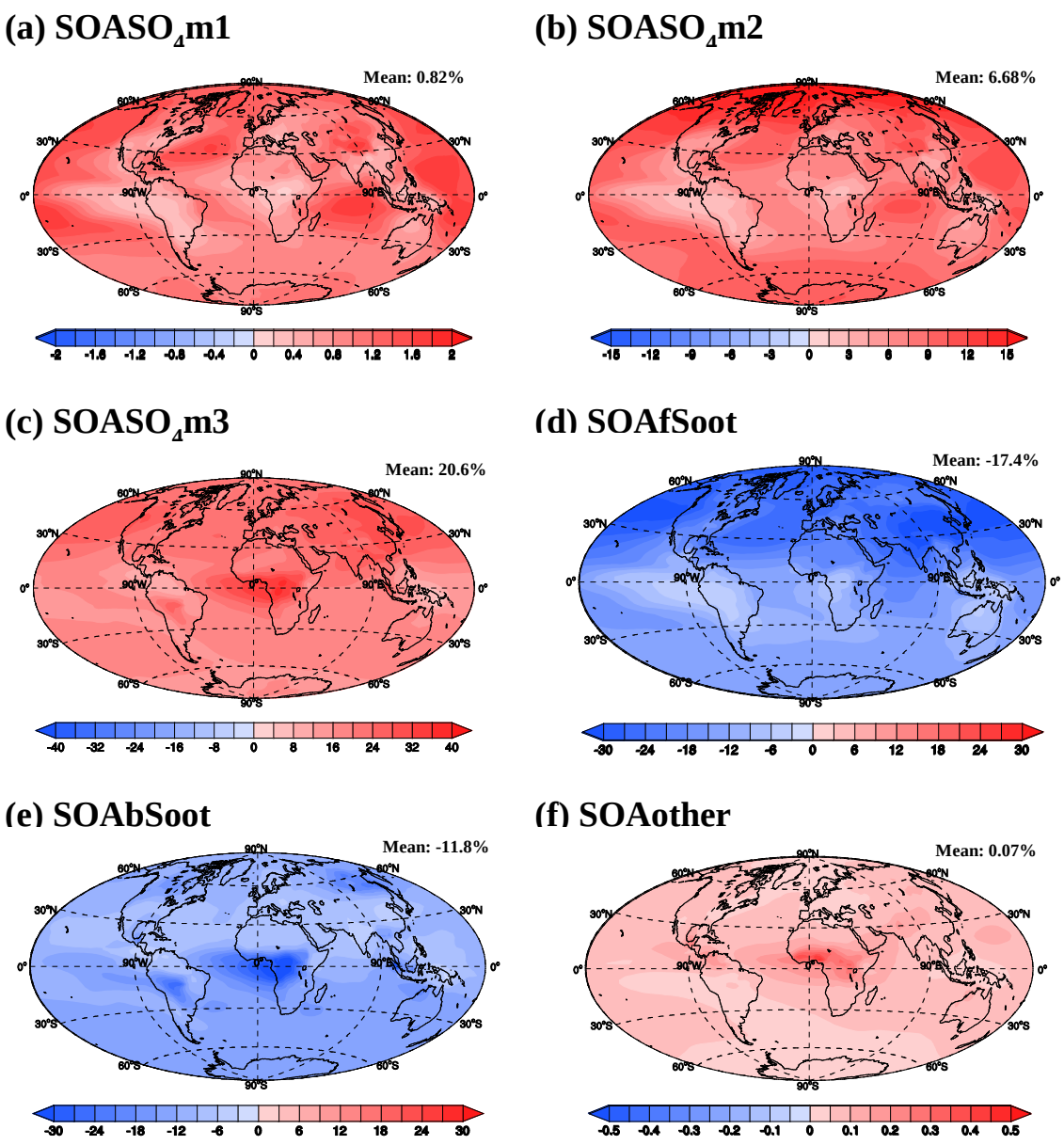

Figure S1. The difference in the percentage of SOA mixed internally with sulfate in the nucleation (a), Aitken (b) and accumulation (c) modes, fSoot (d), bSoot (e) and other aerosols (dust and sea salt) (f) between IM_OC and IM. The global average percentage of the difference of total SOA associated with each aerosol type is shown in each title.

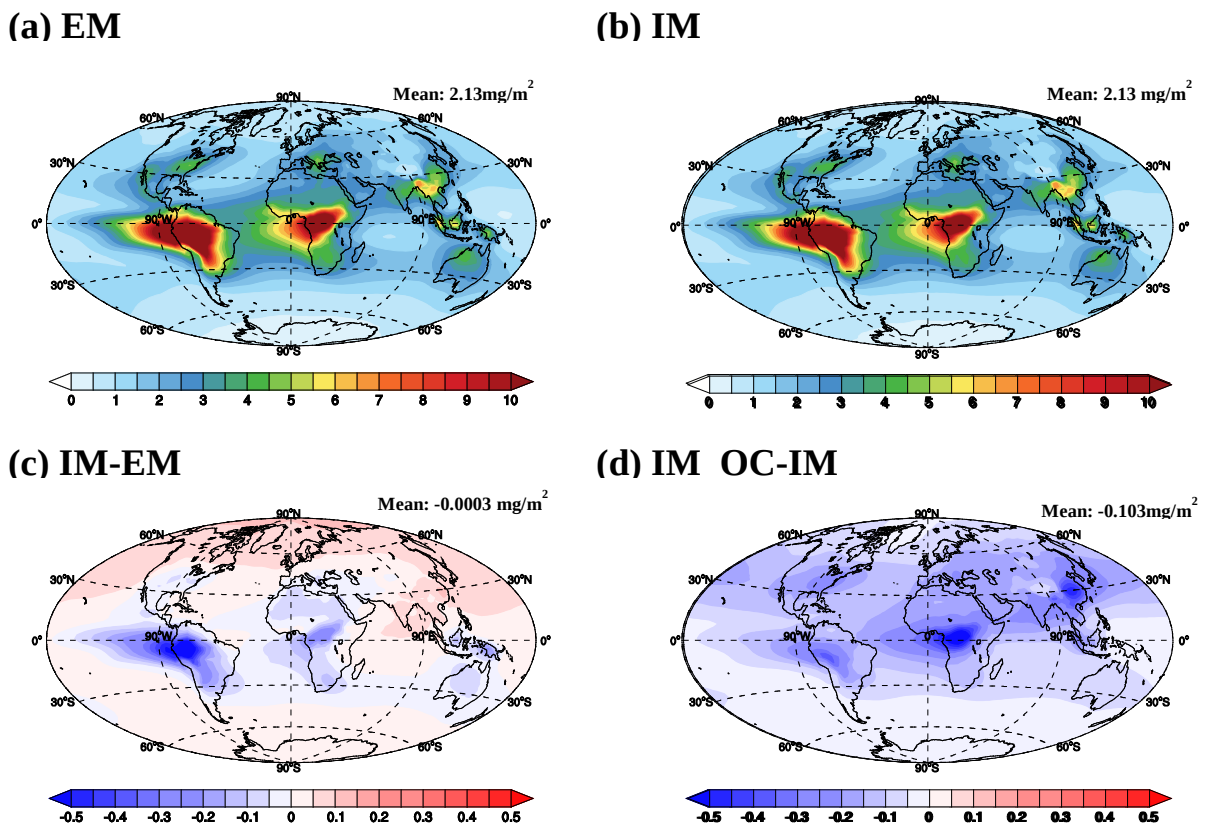

Figure S2. The burden of SOA for the EM (a) and IM (b) schemes. The difference in the SOA burden between IM and EM (c) and between IM_OC and IM (d). The global average SOA burden and difference between schemes is shown in each title.

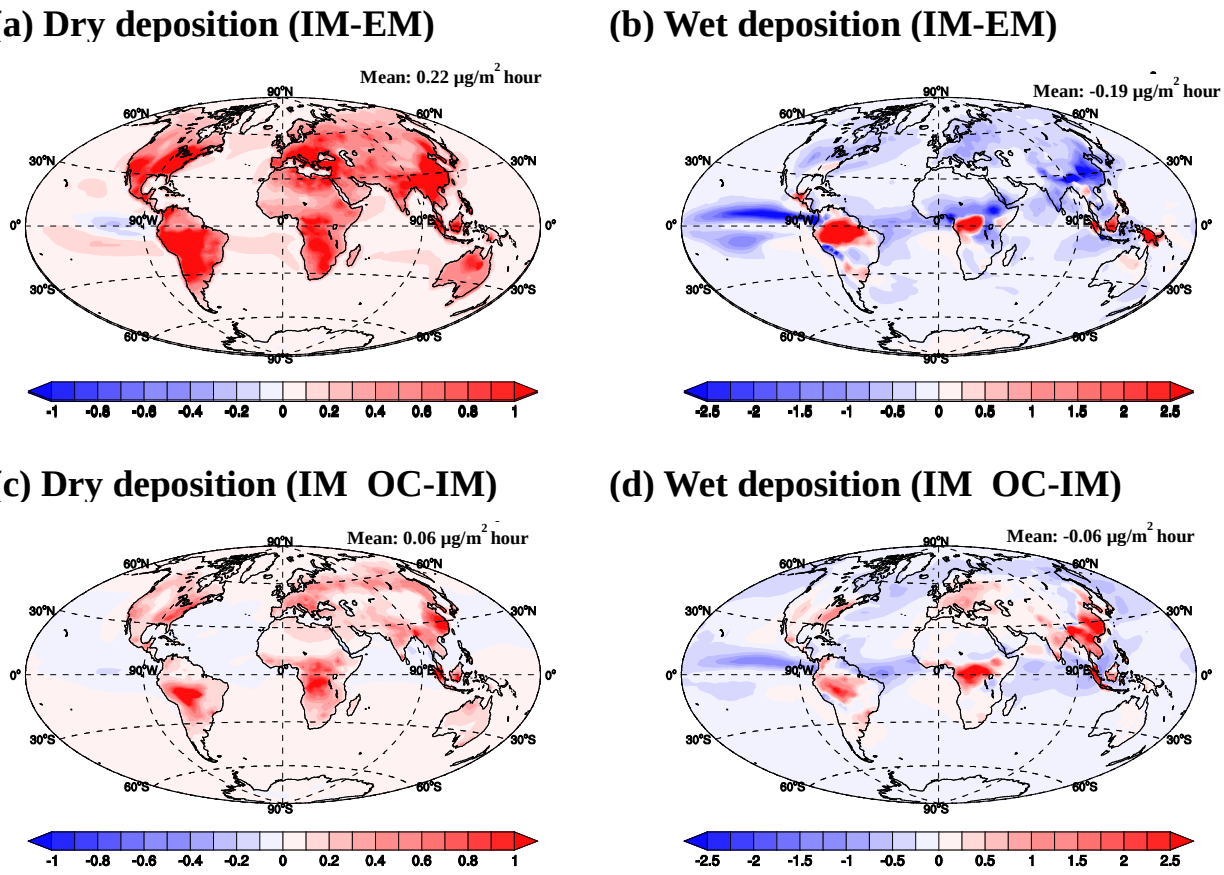

Figure S3. The difference in dry (a) and wet (b) deposition of total SOA between IM and EM. The difference in dry (c) and wet (d) deposition of total SOA between IM_OC and IM. The global average difference in deposition of total SOA is shown in each title.

(a) DRE (IM-EM)

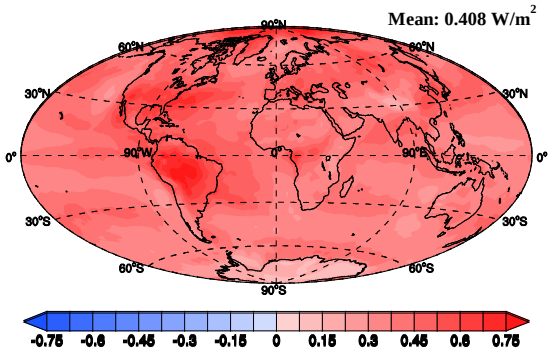

(b) DRE (IM OC-IM)

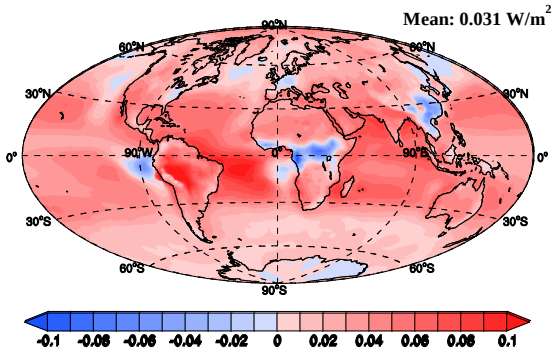

(c) AIE (IM-EM)

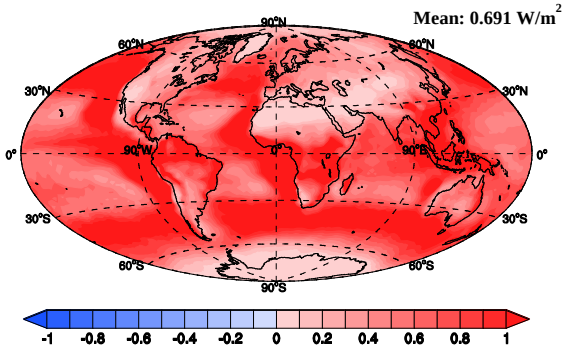

(d) AIE (IM OC-IM)

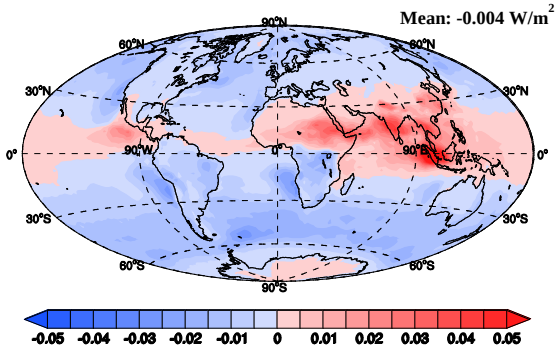

Figure S4. The difference in the DRE between the IM and EM schemes (a) and between IM_OC and IM (b). The difference in the AIE between IM and EM (c) and between IM_OC and IM (d). The global average difference is shown in each title.

(a) IM-EM **(b) IM OC-IM**

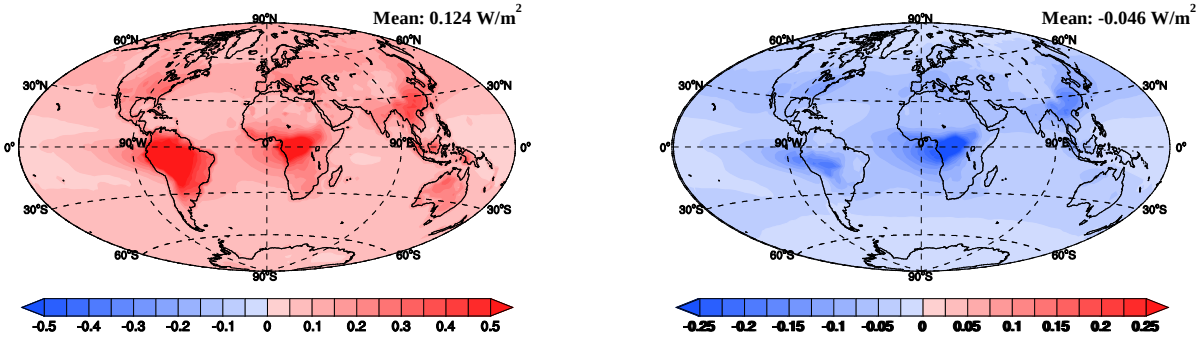

Figure S5. The difference in absorption of radiation due to SOA between IM and EM (a) and between IM_OC and IM (b) (W m^{-2}). The global average difference is shown in each title.

(a) IM-EM **(b) IM OC-IM**

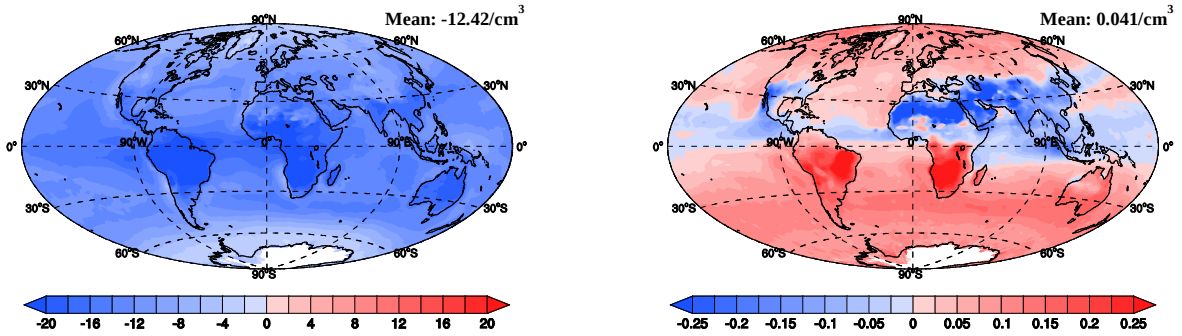

Figure S6. The difference in CDNC at the top of the liquid water clouds due to SOA between IM and EM (a) and between IM_OC and IM (b) (cm^{-3}). The global average difference is shown in each title.

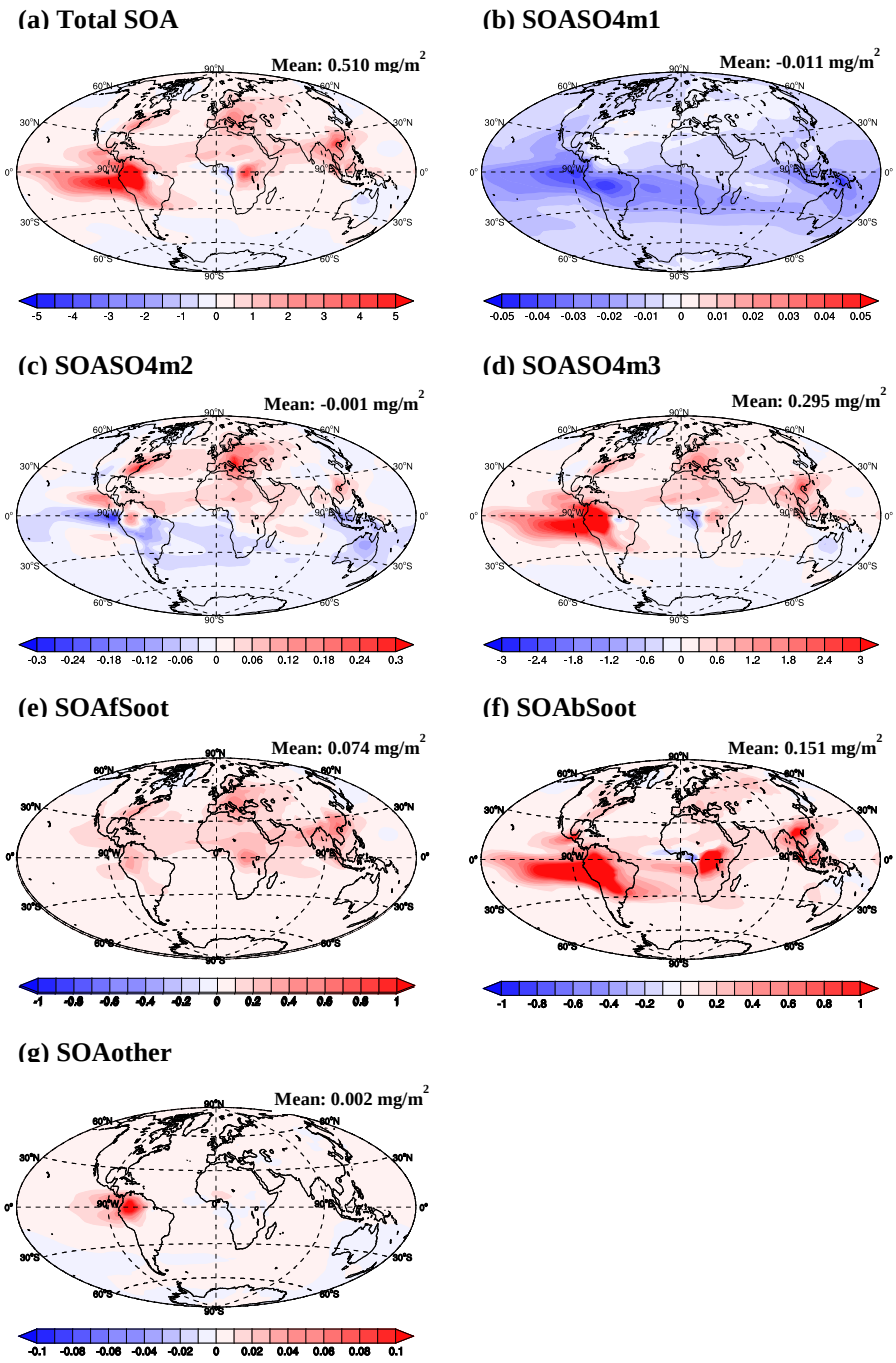

Figure S7. The difference in the future and present day burden of total SOA (a) and SOA internally mixed with sulfate in the nucleation (b), Aitken (c) and accumulation (d) modes, fSoot (e), bSoot (f) and other aerosols (dust and sea salt) (g) in the FUCLI scheme. The global average difference of burden is shown in each title.

(a) Liquid water cloud fraction

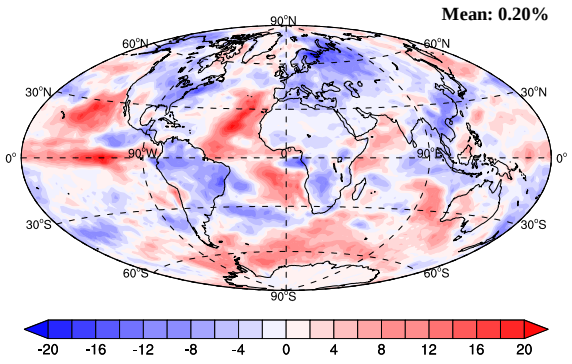

(b) Cloud optical depth

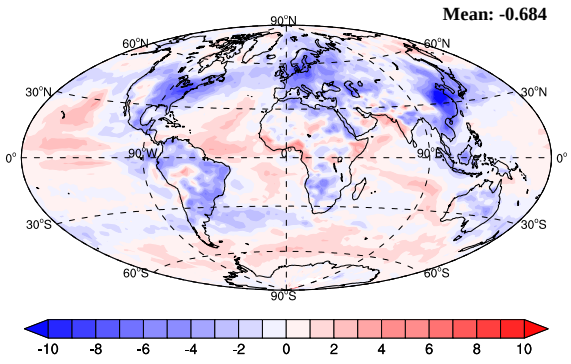

(c) Liquid water path

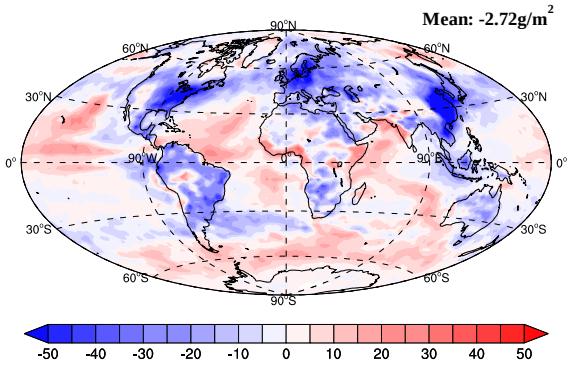

Figure S8. The difference in liquid water cloud fraction (a), grid average cloud optical depth (b) and liquid water path (c) between future and present day. The global average difference is shown in each title.

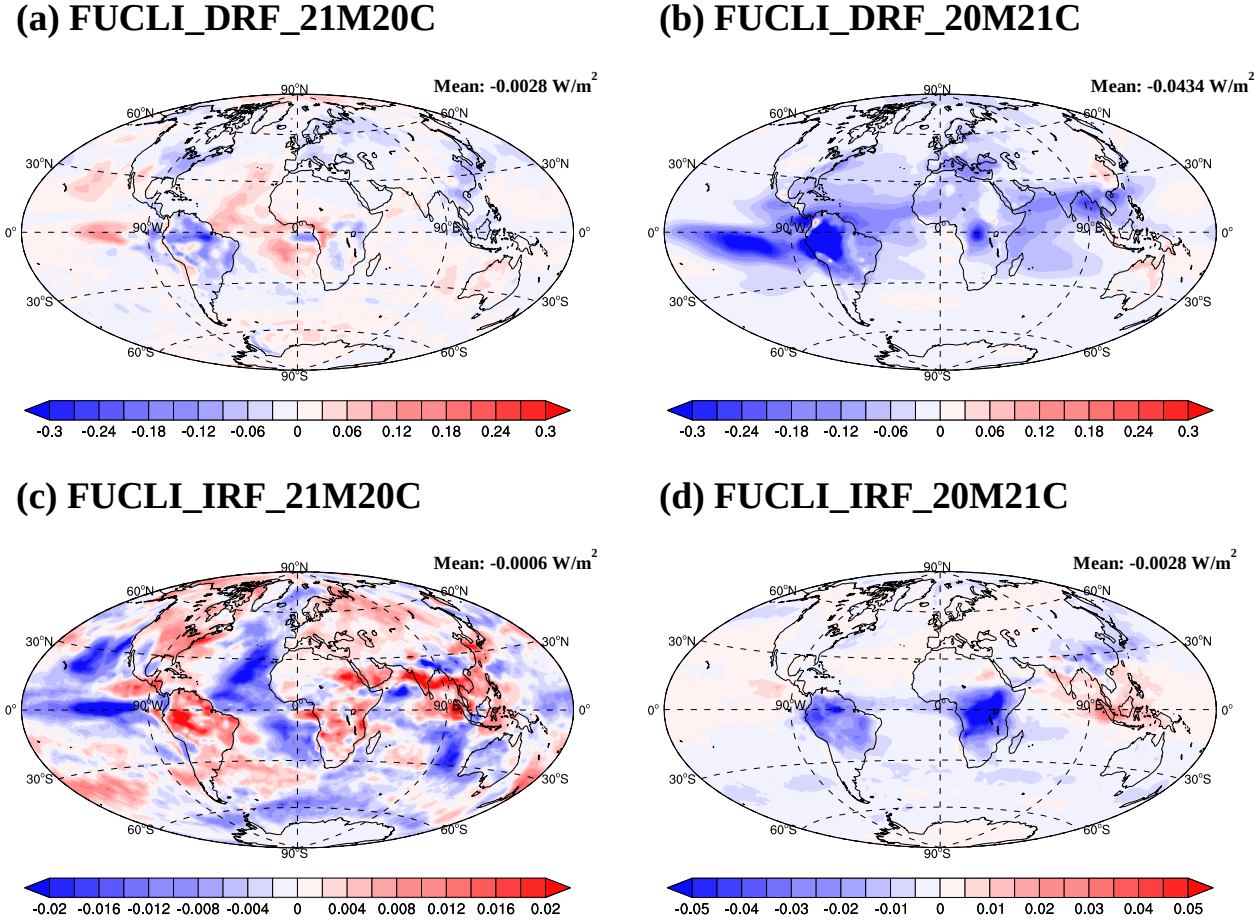

Figure S9. The direct radiative forcing (W m^{-2}) due to changes in the meteorological conditions (a) and SOA concentrations (b) in the future in the FUCLI scheme. The indirect radiative forcing due to changes in the meteorological conditions (c) and SOA concentrations (d) in the FUCLI scheme. The global average radiative forcing is shown in each title.

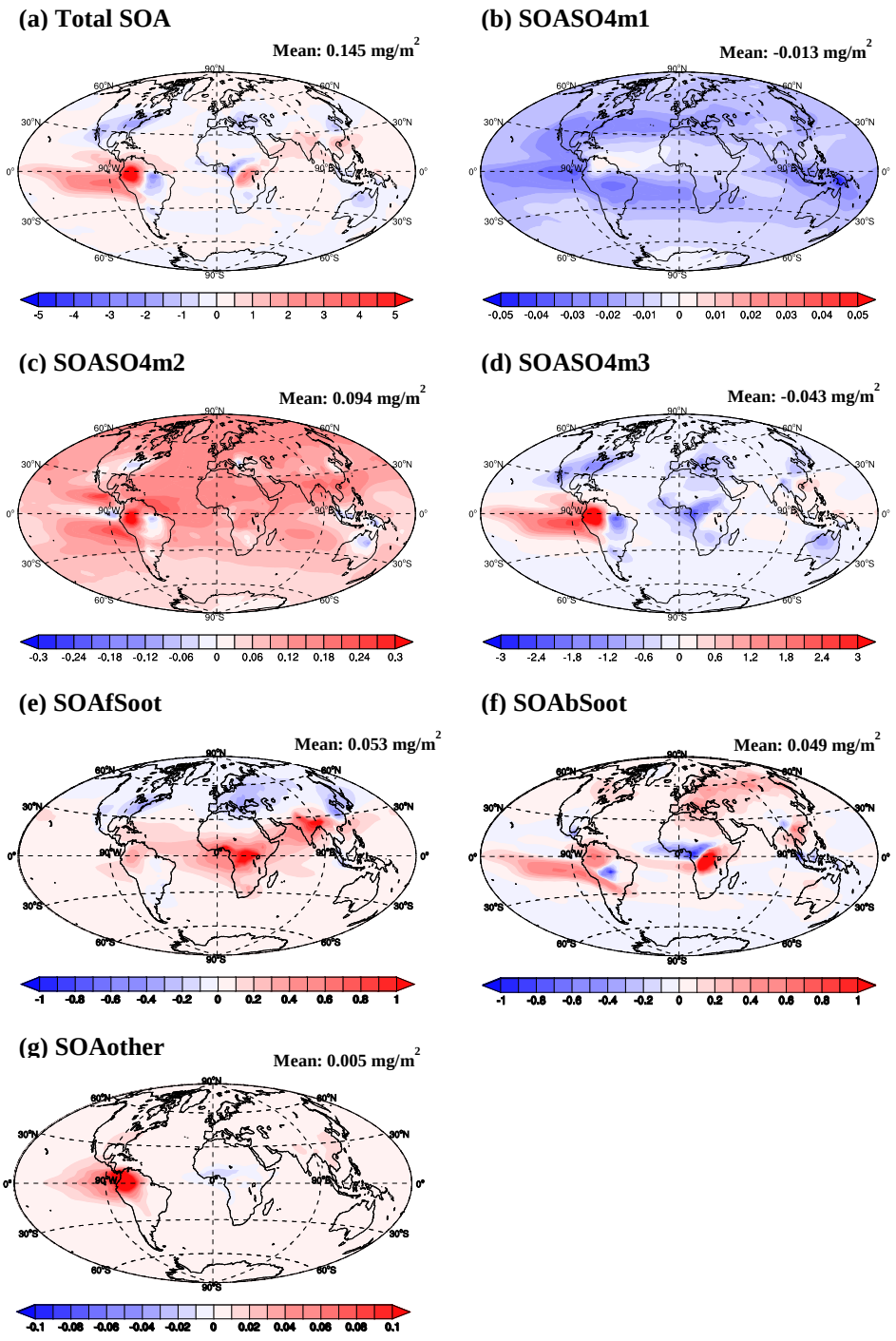

Figure S10. The difference in the future and present day burden of total SOA (a) and SOA internally mixed with sulfate in the nucleation (b), Aitken (c) and accumulation (d) modes, fSoot (e), bSoot (f) and other aerosols (dust and sea salt) (g) in the FUALL scheme. The global average difference of burden is shown in each title.

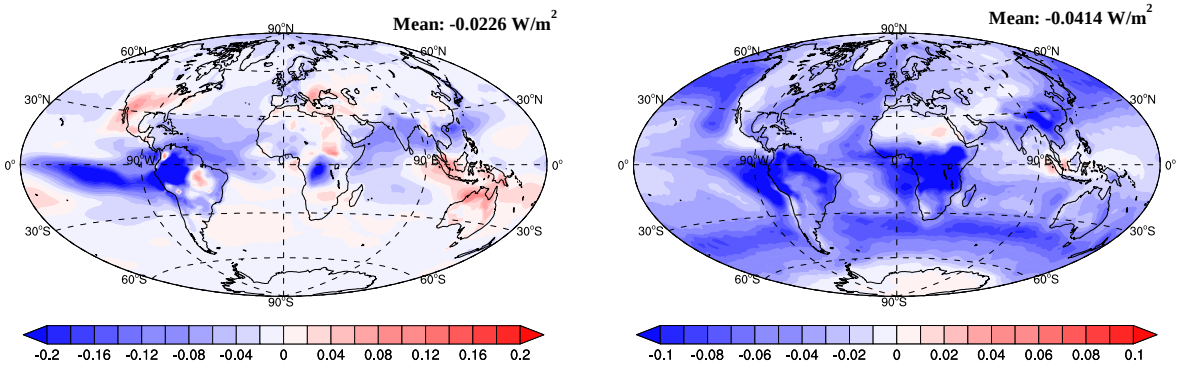

Figure S11. The direct (a) and indirect (b) radiative forcing due to the SOA concentration change in the future in the FUALL scheme (W m^{-2}). The global average radiative forcing is shown in each title.

SI Table

Table S1. Summary of the difference in SOA burden, dry and wet deposition, DRE, AIE, radiation absorption and CDNC among EM, IM and IM_OC schemes

	IM-EM	IM_OC-IM
SOA burden (mg m^{-2})	-0.0003	-0.103
Dry deposition (μg m^{-2} $hour^{-1}$)	0.22	0.06
Wet deposition (μg m^{-2} $hour^{-1}$)	-0.19	-0.06
DRE (W m^{-2})	0.408	0.031
AIE (W m^{-2})	0.691	-0.004
Absorption of radiation (W m^{-2})	0.124	-0.046
CDNC (cm^{-3})	-12.42	0.041